



## ORIGINAL ARTICLE

# Microwave –assisted pyrolysis aspen wood for production of valuable products under different temperatures



Ying Zhang <sup>a</sup>, Song Cheng <sup>b,c,\*</sup>, Bing Wang <sup>d</sup>, Changliang Shi <sup>b,c,\*</sup>, Yanhe Nie <sup>b,c</sup>

<sup>a</sup> School of Emergency Management, Henan Polytechnic University, Jiaozuo 454003, China

<sup>b</sup> College of Chemistry and Chemical Engineering, Henan Polytechnic University, Jiaozuo 454003, China

<sup>c</sup> Collaborative Innovation Center of Coal Work Safety and Clean High Efficiency Utilization, Jiaozuo, 454003, China

<sup>d</sup> Jiangxi HanyaoFu Lithium Technology Co., Ltd, Yichun, 336023, China

Received 20 April 2023; accepted 18 July 2023

Available online 23 July 2023

## KEYWORDS

Aspen wood;  
Microwave heating;  
Pyrolysis product;  
Rhodamine B;  
Energy storage

**Abstract** The valuable pyrolysis products are prepared by pyrolysis of aspen wood using microwave heating at different pyrolysis temperature. High pyrolysis temperature restrains the production of the biochar, and contributes to the generation of the bio-gas. However, pyrolysis temperature has little influenced on the yield of bio-oil. Bio-oil mainly has the phenols, hydrocarbons, ketones, aldehydes and furans compound. The phenols compound of bio-oil generated from 500 °C is 54%. Pyrolysis temperature influences the composition and heating value of bio-gas, and the heating value of bio-gas produced at 700 °C is 13.41 MJ/Nm<sup>3</sup>. Biochar could be used to adsorb Ag<sup>+</sup> from wastewater, which generates value-added A/char after adsorption. Ag<sup>+</sup> adsorption and reduction process are systematically evaluated and analyzed. The generated Ag/char is employed as the catalyst for rhodamine B degradation. Besides, Ag/char has promising application potential in energy storage.

© 2023 The Author(s). Published by Elsevier B.V. on behalf of King Saud University. This is an open access article under the CC BY-NC-ND license (<http://creativecommons.org/licenses/by-nc-nd/4.0/>).

## 1. Introduction

How to reduce the greenhouse gas emissions generation from fossil fuels such as coal and oil consumption is the major challenge of the world. The reduction the greenhouse gas emissions can avoid causing a series of ecological and environmental problems (Yang et al., 2021; Qin et al., 2023a). However, the industry production such as power and chemical products needs the fossil-fuels, which can provide the chemical raw material and energy (Al-Enizi et al., 2020). Therefore, it is urgent to search for the non-fossil fuels to meet the requirement of the industry production and avoid the environmental pollution. Bio-mass has advantages of lost cost, easily available and carbon neutrality, which can be used the renewable carbonaceous resources for

\* Corresponding authors at: College of Chemistry and Chemical Engineering, Henan Polytechnic University, Jiaozuo 454003, China.

E-mail address: [chengsong@hpu.edu.cn](mailto:chengsong@hpu.edu.cn) (S. Cheng).

Peer review under responsibility of King Saud University.



Production and hosting by Elsevier

industry production (Cherubini and Ulgiati, 2010). In addition, biomass can be employed as the feedstock to produce sustainable fuels, and chemicals (Ubaidullah et al., 2021). Pyrolysis is one of the promising biomass conversion method; which can be used to prepared the fuels and chemical products (Al-Enizi et al., 2020). What's more; pyrolysis is more favorable for large-scale applications (Foong et al., 2020).

Microwave heat is the promising heating method, which has benefits of selective and non-contact heating, and energy saving (Tang et al., 2020; Cao et al., 2020). Microwave heat can be employed in biomass pyrolysis due to fact that it can process a variety of biomass (Chen et al., 2016). Microwave heat is conducive to production of high-quality liquid and gas fuel in the biomass pyrolysis process (Qin et al., 2023b). Besides, biomass with high moisture can contribute to improving its microwave adsorption capacity, which realizes the rapid heating of biomass during pyrolysis process (Cheng et al., 2017; Cheng et al., 2021). Microwave heat is proved at both pilot scale and industrial scale for processing various biomass (Abdelsayed et al., 2018). Hot spots are generated in the microwave heat process. The yield and qualities of the products are significantly influenced by hot spots during pyrolysis process (Zhang et al., 2017). The empty oil palm can produce bio-oil with 74% of phenolic compounds by pyrolysis using microwave heat (Prashanth et al., 2020). Gautam et al. (2019) pointed out that bio-oil produced from macroalgae has little oxygen containing compound when microwave heat processes the macroalgae (Gautam et al., 2019). Parvez et al. (2019) reported that microwave heat produces a lot of H<sub>2</sub>, which is 15% more than conventional heat (Parvez et al., 2019). So; microwave heat has promising application potential in biomass pyrolysis.

The physicochemical properties and yield of the pyrolysis products are significantly influenced by the pyrolysis conditions such as pyrolysis temperature, pyrolysis time and particle size of feedstock (Yek et al., 2021). Pyrolysis temperature is an important pyrolysis index among pyrolysis parameters (Yek et al., 2021). The large yield of the bio-char is produced at low pyrolysis temperature ( $\leq 400$  °C). Moderate pyrolysis temperature (400–600 °C) is beneficial for the production of bio-oil (Wang et al., 2022; Nishu and Liu, 2022). Besides, desire pyrolysis temperature produces large energy-density of bio-oil and bio-gas, which could be used as the bioenergy (Aysu and Durak, 2015).

Aspen wood, called as the poplar, is acted as feedstock to prepare valuable products by microwave-assisted pyrolysis. Ag<sup>+</sup> is one of the harmful metal ions, which must be removed from wastewater. Biochar is an important pyrolysis product, which can be used in the wastewater treatment and energy storage (Table S1). Physicochemical property and yield of the pyrolysis products at 400–800 °C are investigated, and then the prepared biochar is used for Ag<sup>+</sup> removal. However, the biochar forms the Ag@Biochar (A/char) after Ag<sup>+</sup> adsorption. A/char can be used in rhodamine B degradation from wastewater and energy storage. The main tasks of this work are: (1) to investigate the physicochemical property and yield of the pyrolysis products at 400–800 °C; (2) to investigate the formation process of the A/char; (3) to analyze rhodamine B removal and energy storage potential using A/char.

## 2. Experimental and method

### 2.1. Materials

Aspen wood (AW) is collected from Jiangsu province, China. Rhodamine B and silver nitrate and are purchased from the Sinopharm Chemical Reagent Co. Ltd., China. Moisture, ash, volatile matter and fixed carbon of AW are 10.37 wt%, 1.42 wt%, 74.30 wt% and 13.91 wt%, respectively. The C, H, N and O element of the AW are 42.14 %, 6.21%, 10.86 % and 50.79 %, respectively. The biochemical composition

of AW is cellulose of 39.00%, hemicellulose of 36.40%, lignin of 19.30 % and other of 5.30%.

### 2.2. Pyrolysis method

Multimode microwave furnace is employed in pyrolysis experiment system with the output power of 0–3 KW and the microwave frequency of 2.45 GHz. Pyrolysis temperature is 400–800 °C with the pyrolysis time of 30 min in the pyrolysis experiment process. Pyrolysis gas is taken out using nitrogen. The glass condensers are used to condense to obtain bio-oil and bio-gas. The liquid is bio-oil, which is collected from glass condensers. Bio-gas is non-condensing components of pyrolysis gas. The bio-gas is pre-dry using the drying tube before analysis. Biochar is pyrolysis residue of the biomass in microwave furnace.

### 2.3. Characterization

Gas chromatography (GC-Tracel310) is used to analyze the bio-gas. GC-MS is employed to detect the chemical composition of bio-oil. Pore structure of biochar is analyzed using Autosorb instrument (Hou et al., 2022). Scanning electronmicroscopy is employed to analyze the surface microstructures. Ramascope spectroscopy is used to analyze the biochar. X-ray diffraction (XRD) analysis is used to test biochar (Cheng et al., 2023). X-ray photoelectron spectroscopy (XPS) is employed to detect the surface chemical properties of biochar. The chemical property of biochar is detected by the Fourier transform infrared spectroscopy.

## 3. Results and discussions

### 3.1. Heating curves of AW

The AW heating curves at 1000–2000 W are shown in Fig. 1a. As Fig. 1a shown, the heating curves of AW at 100–2000 W have similar trend. However, it has different heating rates. The AW heating rate of 1000 W is low compared to that of the 1500 W and 2000 W. It can be explained that it produces little microwave energy at 1000 W. Therefore, it need long time to obtain the microwave energy to reach 800 °C. Fig. 1a indicates that heating time of AW is 16 min to reach 800 °C at 1000 W. However, AW takes 7 min to reach 800 °C at 2000 W. It can obtain the conclusion that large microwave power contributes to AW heating and reduces heating time. The heating curve of AW at 1500 W is used to analyze the heating process of the AW. As Fig. 1a shown, AW has slowly heating rate before 200 °C due to fact that AW has poor dielectric property. The hemicellulose and cellulose of AW slowly decompose and the preliminary biochar skeleton is subsequently formed as heating time increases. The hemicellulose and cellulose of the AW are rapidly decomposed or depolymerized, which produces low molecular weight volatiles. Besides, lignin begins to decompose after 400 °C. Biochar is generally formed as pyrolysis temperature increases, which has good dielectric properties. Therefore, the heating rate of AW rapidly increases in later heating period. AW has large heating rate at 1500 W. So, pyrolysis experiment is conducted in 1500 W. Fig. 1b shows the dielectric property of AW. The

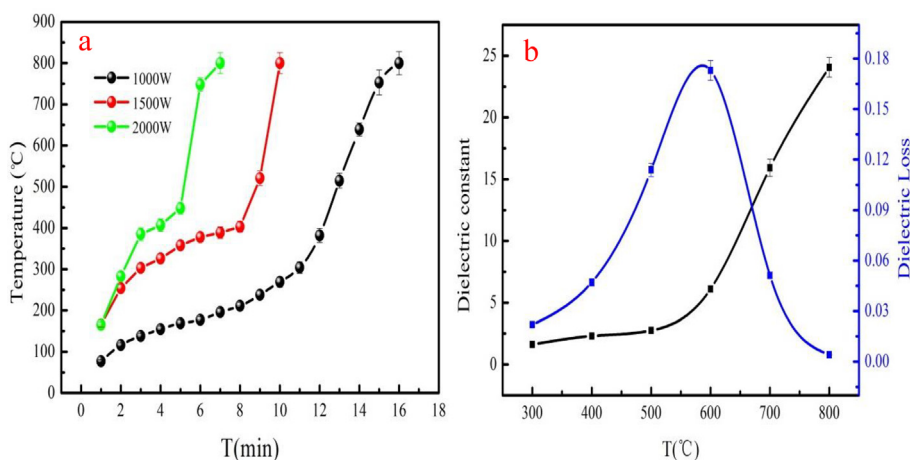


**Fig. 1** The dielectric property (a) and heating curves (b) of AW.

**Table 1** Compositions of bio-oil at 400–800°C.

Item	Components	400 °C	500 °C	600 °C	700 °C	800 °C
		Relative content (%)				
1	Cyclohexan-1,4,5-triol-3-one-1-carboxylic acid	0.56	0.75	0.83	1.00	0.34
2	Dihydroxyacetone	–	0.43	0.28	0.83	–
3	2-Methoxytetrahydrofuran	3.07	3.64	3.96	3.7	1.01
4	Cyclobutene, 2-propenylidene-	0.91	0.74	0.63	1.84	2.25
5	Ethane, 1,1,1-trimethoxy-	–	–	–	5.02	3.99
6	Butanoic acid	0.21	1.57	0.84	0.51	0.96
7	Cyclopentanone	2.83	1.42	0.51	–	–
8	2-Propanone, 1,1-dimethoxy-	–	0.34	0.5	2.2	5.46
9	Ethane, 1,1,2-trimethoxy-	–	–	2.25	3.43	–
10	Furfural	9.47	8.28	5.25	2.97	8.46
11	(Z)-3-Pentenoic acid, methyl ester	–	–	–	1.09	1.54
12	1,1,3-Trimethoxy propane	1.55	–	–	–	–
13	Ethylbenzene	2.76	3.79	2.29	–	–
14	p-Xylene	5.18	5.80	4.36	0.46	15.68
15	Furan, tetrahydro-2,5-dimethoxy-	14.55	11.85	17.03	10.07	5.95
16	Benzene, 1,3-dimethyl	2.08	2.58	1.95	15.22	7.51
17	1-(Furan-2-yl)-4-methylpentan-1-one	0.72	–	–	–	–
18	F3(2H)-Furanone, dihydro-5-isopropyl-	–	–	–	0.41	0.64
19	6-Hydroxy-2,6-dihydropyran-3-one	–	–	0.36	0.72	0.23
20	enzene, 1,1'-dodecylidenebis[4-methyl-	0.23	0.52	–	–	–
21	1,7-Heptanediol	0.54	–	–	–	–
22	Furan, tetrahydro-2,5-dimethoxy-	3.07	5.02	8.79	–	–
23	Ethanone, 1-(2-furanyl)-	0.92	0.8	1.23	–	1.28
24	2H-Pyran, 3,4-dihydro)	–	–	–	–	0.55
25	Benzenepropanoic acid, α,α-dimethyl-	–	–	–	–	0.75
26	2-Oxepanone, 7-methyl-	0.14	0.35	1.41	–	–
27	Glycolaldehyde dimethyl acetal	–	–	0.88	0.47	0.29
28	Phenol	42.71	47.66	36.95	6.09	–
29	Benzofuran	–	–	0.58	0.81	–
30	2-methyl- Phenol	3.95	2.18	1.87	0.90	–
31	p-Cresol	1.54	1.35	–	–	–
32	2-methoxy-Phenol	4.35	2.42	2.89	–	–

dielectric constant of AW is slow increase at 400–800 °C (Fig. 1b). Besides, the dielectric loss of AW is also general increase before 600 °C. Dielectric property of AW is in good agreement with heating curves analysis.

### 3.2. Influence of pyrolysis temperature

Fig.S2 shows the pyrolysis products distribution at 400–800 °C. As Fig.S2 shown, the low pyrolysis temperature

contributes to the generation of bio-oil. This phenomenon can be explained that the generated microwave energy is used for AW pyrolysis, and the produced volatile component generates the bio-oil (Wang et al., 2016). The yield of the bio-oil decreases from 24.87% to 18.40% at 500–800 °C. Wang et al. (2016) pointed out that the gaseous product is quickly generated, while bio-oil is restrained at high pyrolysis temperature (Zhang et al., 2010). As Fig.S2 shown, bio-gas yield is general increase at 400–800 °C. It can be explained that high pyrolysis temperature is conducive to the production of the bio-gas. While the yield of the biochar is decrease at 400–800 °C. The minimum yield of the biochar is 21.20%. The reason might be that high pyrolysis temperature converts portion of biochar into bio-gas. Therefore, 500 °C is the desire pyrolysis temperature because of large yield of the bio-oil.

### 3.3. Pyrolysis products investigation

#### 3.3.1. Bio-oil investigation

Table 1 presents the bio-oil composition. As Table 1 shown, the composition of the bio-oil is diverse. However, the bio-oil contains hydrocarbons, ketones, aldehydes, phenols and furans. Therefore, bio-oil is classified into above five groups. As Fig. S3 shown, pyrolysis temperature affects main components content of bio-oil. Bio-oil has large content of the phenolic compound compared to other compounds. It can be explained by the secondary transformation, which promotes

to generate the phenolic compound. Besides, interaction of moisture/steam with formed aromatics also contributes to generating phenolic compound (Mukarakate et al., 2015). The generated phenolic compound can be used as the precursor to produce the chemical and pharmaceutical with large economic benefits.

However, bio-oil still has poor performance such as low pH and high O content. Therefore, pre-processing of bio-oil is necessary after pyrolysis. The thermal steam filtration and catalytic modification are the common pre-processing method to improve its physicochemical properties (Han et al., 2019).

#### 3.3.2. Bio-gas investigation

Kabir et al. (2018) pointed out that the involved generation reactions of bio-gas are complex (Kabir et al., 2018). The main reactions of the bio-gas generation are depolymerization, fragmentation and secondary reactions (KristinaMaliutina and JianglongYu, 2017). Fig. S4a presents the component of the bio-gas at 400–800 °C. The bio-gas produced at low temperature has large content of CO<sub>2</sub>. However, CO<sub>2</sub> content gradually decreases with increasing in temperature. CO<sub>2</sub> content reaches the minimum value at 800 °C, indicating that generation reactions of CO<sub>2</sub> are hindered at high temperature. The CO content decreases before 500 °C and subsequently increases at 500–800 °C due to fact that cellulose and hemicellulose easily lose decarboxylation and then convert into CO. H<sub>2</sub> content gradually increases as pyrolysis temperature increases.

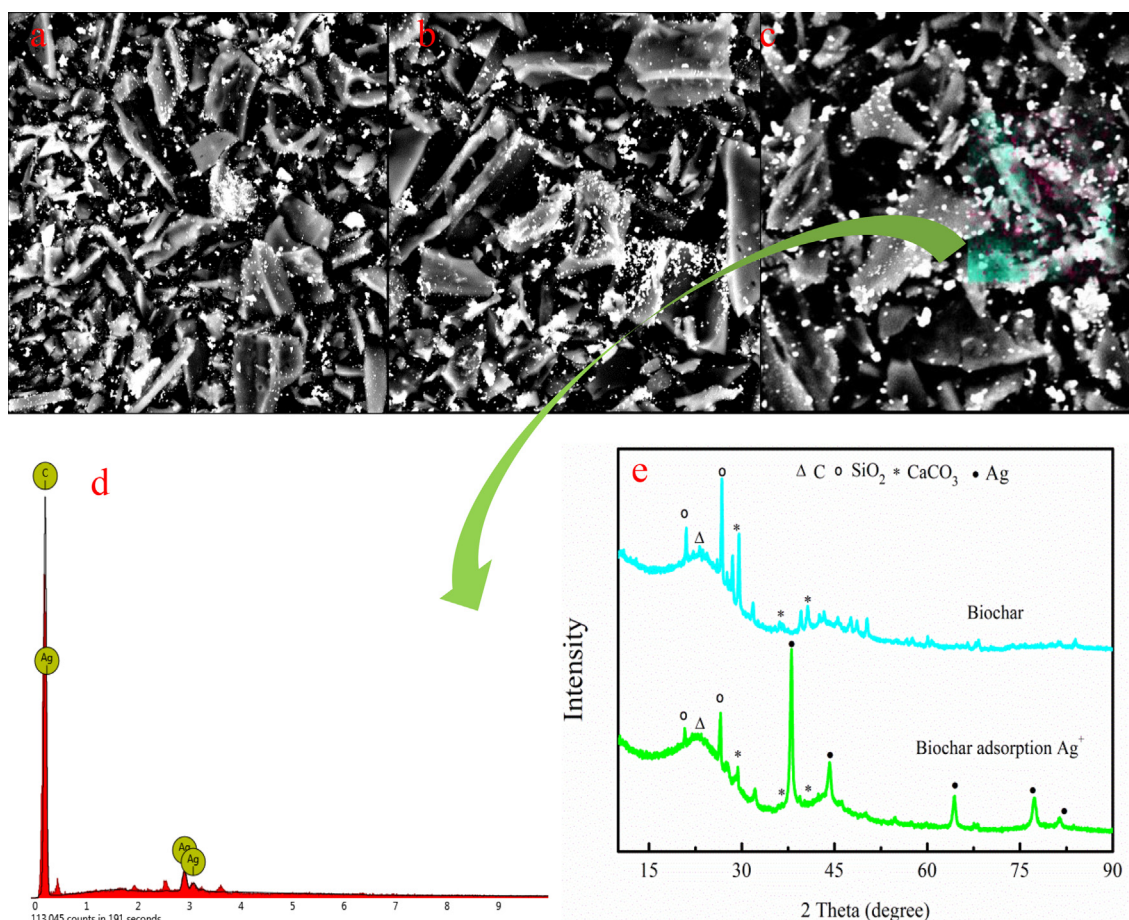


Fig. 2 SEM-EDS images of biochar after adsorption of Ag<sup>+</sup> (a-d), XRD spectra of biochar before and after Ag<sup>+</sup> adsorption (e).



The  $H_2$  content reaches the maximum value of 41.07% at 800 °C, indicating that high pyrolysis temperature contributes to  $H_2$  production.  $CH_4$  content is increase at 400–700 °C, which is increase from 4.76 % to 13.07 %. However,  $CH_4$  content decreases at 700–800 °C. The pyrolysis temperature significantly influences the component of the bio-gas (Zhang et al., 2018; Foong et al., 2020). Bio-gas heating value generally increases at 400–800 °C (Fig. S4b). As Fig. S4b shown, the maximum heating value of bio-gas is 13.42 MJ/Nm<sup>3</sup>. However, the bio-gas heating value is low compared to the marsh gas and

natural gas, which limits it large scale application (Zhang et al., 2018). Conversion  $H_2$  /CO into  $CH_4$  and reduction  $CO_2$  content can increase the heating value of the bio-gas.

### 3.3.3. Biochar investigation

Biochar produced from different temperature has abundant pore structure. The range of specific surface area of biochar produced at 400–800 °C is 86.59–293.84 m<sup>2</sup>/g. Bio-char produced from 700 °C has large surface area. It can be explained

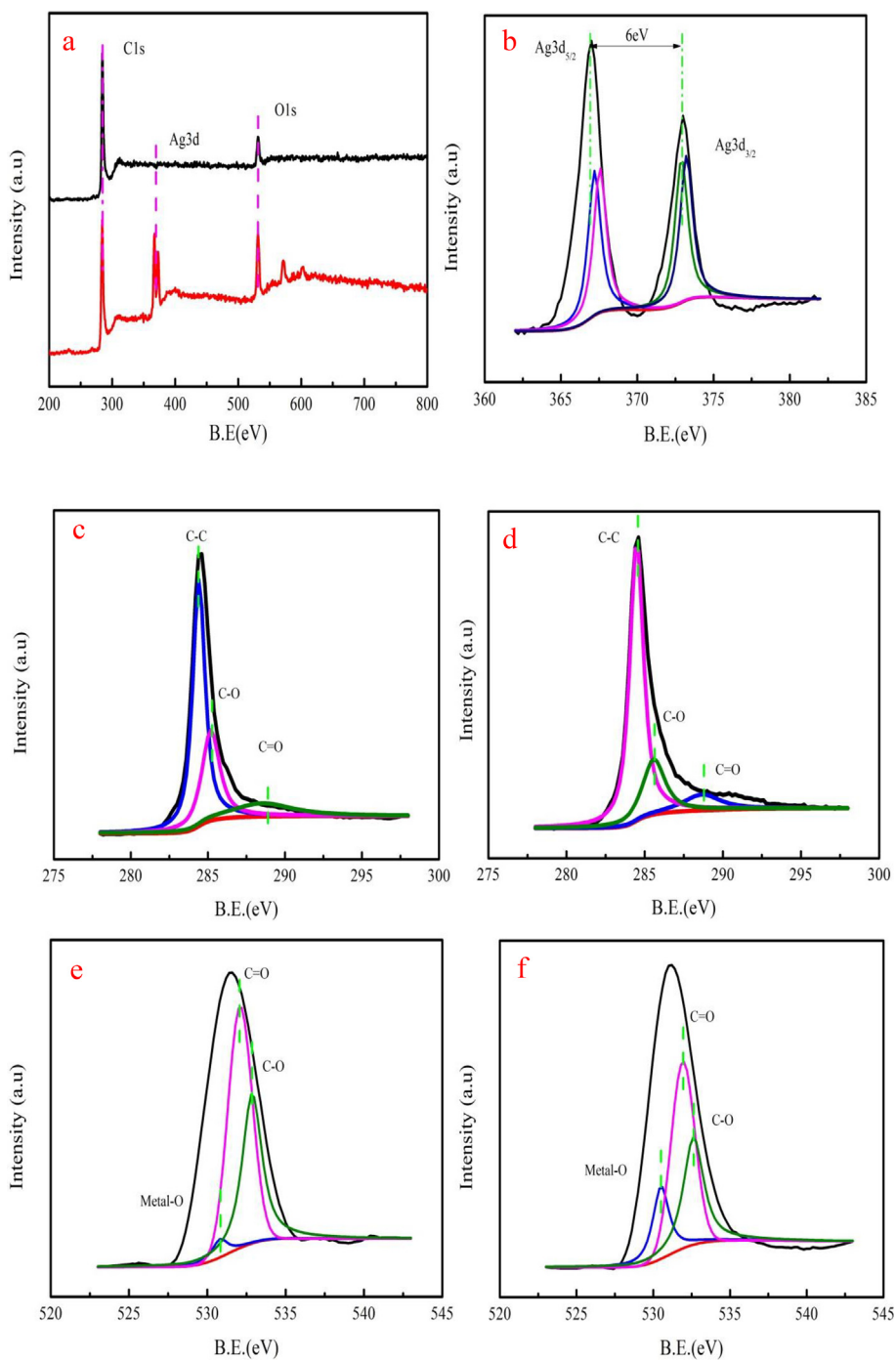


**Fig. 3** The wide scan XPS spectrum biochar before and after (a), Ag 3d spectra of (b), C1s spectra of (c-d) and O1s spectra of before and after adsorption (e-f).

that high pyrolysis temperature is conducive to forming pores. However, if the pyrolysis temperature is too high, the generated pore will be ruined. It is the reason why the surface area of biochar produced at 800 °C decreases. The above analysis demonstrates that pore structure of biochar is also influenced by pyrolysis temperature. Fig.S5 shows the SEM images of biochar prepared from 400 to 800 °C. Fig.S5 indicates that the biochar prepared from 400 to 500°C has underdeveloped pores or little pore. However, a huge number of pores are appeared as pyrolysis temperature increases. It can be explained that high pyrolysis temperature contributes to the formation of pore. The SEM analysis is in good agreement with pore structure analysis.

Raman spectrum of biochar is shown in Fig.S6. As Fig.S6 shown, biochar has two peaks at around 1350 and 1600  $\text{cm}^{-1}$ , which are named as D peak and G peak. D peak means the defection of crystalline structure. While, G peak is used to describe the graphitic structure. Graphitization degree of biochar is investigated by  $I_D/I_G$  value. As Fig.S7 shown, the  $I_D/I_G$  value increases as pyrolysis temperature increases.

### 3.4. Application of biochar

#### 3.4.1. $\text{Ag}^+$ adsorption of biochar

The scholars reported that biochar has abundant chemical functional groups, which can be used in wastewater treatment (Alshawi et al., 2022; Mohammed et al., 2022; Cheng et al.,

2022). Biochar prepared from 700 °C is used for  $\text{Ag}^+$  adsorption because of large BET surface area for evaluation its adsorption performance. The detailed information of adsorption process is in the Supplementary materials.  $\text{Ag}^+$  adsorption capacity of the biochar is tested using adsorption experiment. The residual concentration is detected by atomic absorption spectrum after adsorption equilibrium. The amount of the adsorbed  $\text{Ag}^+$  on biochar is 65.14 mg/g based on adsorption experiment.

#### 3.4.2. $\text{Ag}^+$ adsorption and reduction process

SEM-EDS images of biochar after  $\text{Ag}^+$  adsorption are presented in Fig. 2. Fig. 2a-b indicates that the surface of biochar has many white particles. The white granular is silver element according to EDS analysis (Fig. 2c-d). XRD is employed to further analyze the particle matter. As Fig. 2e shown, the surface of the original biochar has the  $\text{SiO}_2$  and  $\text{CaCO}_3$ . However, the silver crystal exists on biochar after  $\text{Ag}^+$  adsorption. The existence of metallic silver demonstrates that  $\text{Ag}^+$  is converted into the metallic silver by reduction after adsorption. The value-added A/char is generated on biochar after  $\text{Ag}^+$  adsorption based on XRD/SEM-EDS analysis.

XPS spectrum is employed to investigate  $\text{Ag}^+$  adsorption and reduction process. As Fig. 3 a shown, biochar appears Ag element. The  $\text{Ag}3d_{3/2}$  and  $\text{Ag}3d_{5/2}$  are appeared in Ag spectra, indicating that silver has two different status on biochar, corresponding to the form of metallic silver ( $\text{Ag}3d_{5/2}$ ) and

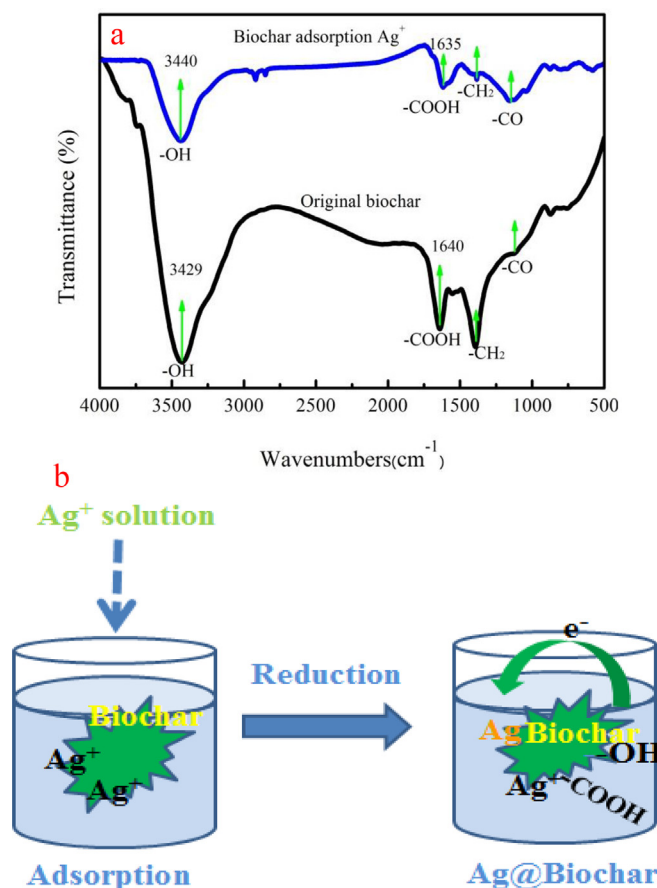


Fig. 4 FTIR spectra of original biochar before and after  $\text{Ag}^+$  adsorption (a), adsorption and reduction process of  $\text{Ag}^+$  (b).

$\text{Ag}^+$  ( $\text{Ag}3d_{3/2}$ ), respectively. Binding energy distance of two different states of Ag is 6.0 eV. The peak area of  $\text{Ag}3d_{5/2}$  is large compared to  $\text{Ag}3d_{3/2}$  (Li et al., 2019). This result proves that Ag ions are converted into silver by reduction. As Fig. 3c-d shown, C1s spectra of biochar contain C—C, C—O, and C=O groups. However, binding energies and peak areas of above groups have changed after  $\text{Ag}^+$  adsorption. C—O and C=O peak area decrease by 7.67% and 4.14% after  $\text{Ag}^+$  adsorption, respectively. XPS analysis indicates that hydroxyl and carboxylic groups of biochar involves in  $\text{Ag}^+$  adsorption. O1s peaks of biochar before and after adsorption are also employed to further investigate  $\text{Ag}^+$  adsorption process (Fig. 3e-f). C=O and C—O peak area decrease by 8.31 % and 6.28 % after  $\text{Ag}^+$  adsorption, respectively. O1s peak analysis is in good agreement with C1s peak analysis. The metal-O group peak area increases by 14.32%, demonstrating that biochar appears Ag element. The binding energy of the metal-O group is 530.81 eV before adsorption. However, it is shifted to 531.05 eV. It can be explained that the donation of lone electron pair is generally low compared to electron density around oxygen atom (Zhang et al., 2019). Therefore; the binding energy of O1s increases. Fig. 4a indicates that the—OH group is appeared near  $3440\text{ cm}^{-1}$ . The —COOH group is found biochar at around  $1640\text{ cm}^{-1}$ . Besides, the C—O peak is found at the peak near of the  $1130\text{ cm}^{-1}$ . The peak intensity

and location of —OH and —COOH groups are changed after  $\text{Ag}^+$  adsorption based on FTIR spectra analysis.

$\text{Ag}^+$  reduction process can be described that carboxyl and hydroxyl groups reduce  $\text{Ag}^+$  into the metastable Ag clusters on biochar because of lower surface energy (Abbas et al., 2020). The generated Ag clusters are thermodynamically far more favored than smaller entities. The metastable silver clusters generally agglomerate and subsequently form A/char during growth period (Zhao et al., 2018). The above analysis results demonstrate that  $\text{Ag}^+$  ions are converted into Ag nanoparticles on biochar after adsorption. Fig. 4b presents the  $\text{Ag}^+$  adsorption and reduction process. The application of A/char in dye removal and energy storage is also investigated.

### 3.4.3. Rhodamine B degradation performance of A/char

Rhodamine B is employed to investigate the degradation performance of the A/char in condition of  $\text{NaBH}_4$ . 50 mL rhodamine B solution at 20–40 mg/L is mixed with the 0.02 g A/char. The detailed information is in the supporting material. The rhodamine B degradation removal ( $\eta$ ) of A/char and biochar with or without  $\text{NaBH}_4$  is presented in Fig. 5a-b. The  $\eta$  is general increase as degradation time increases at 20–40 mg/L (Fig. 5a). The maximum  $\eta$  of A/char is 81.75% at rhodamine

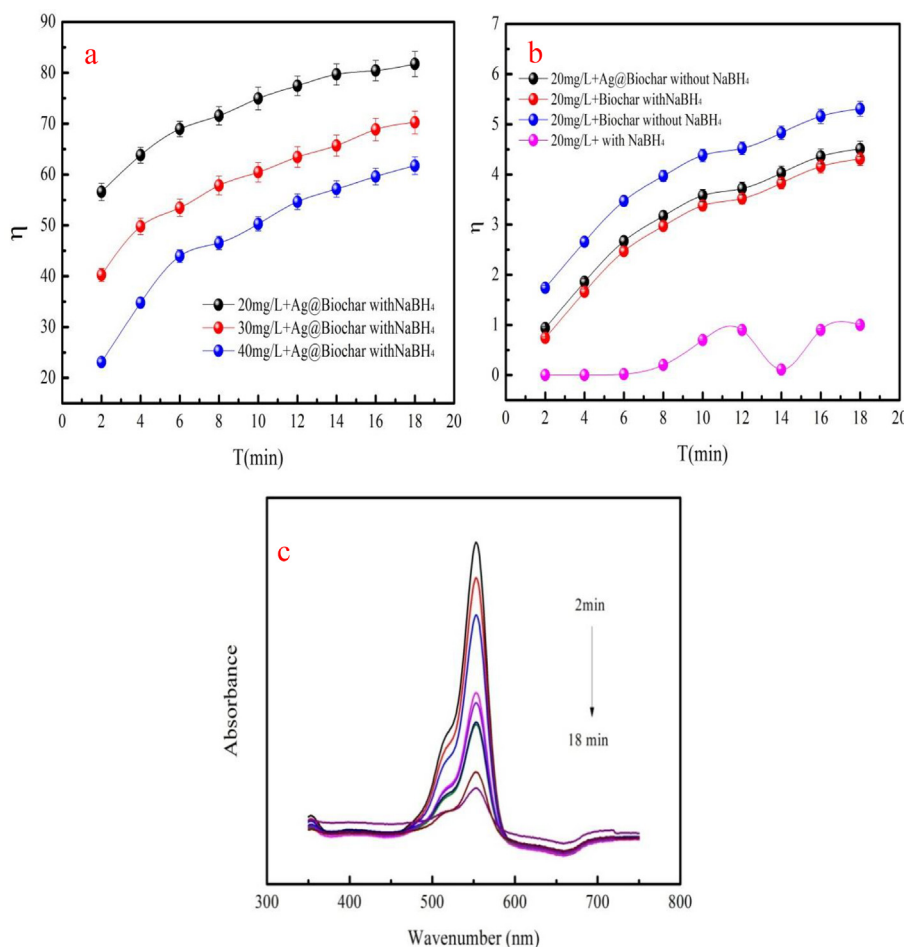


**Fig. 5** The degradation removal of rhodamine B using Ag/char with  $\text{NaBH}_4$  (a), degradation removal of rhodamine B using biochar and A/char with or without  $\text{NaBH}_4$  (b) and UV-visible absorption spectra of rhodamine B of A/char at 20 mg/L (c).

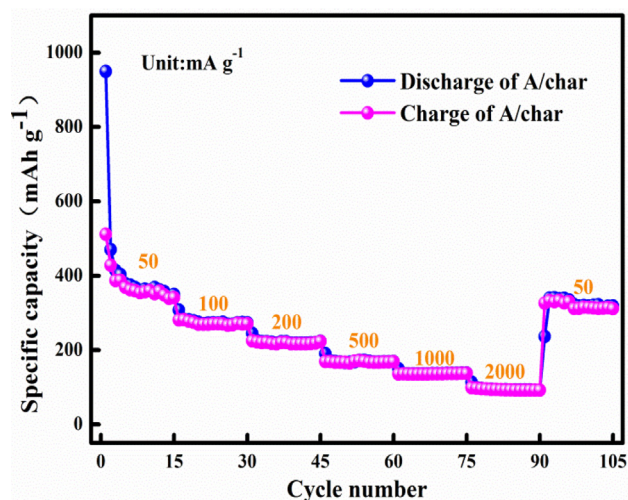


Fig. 6 Rate performance of A/char for the lithium ion batteries at different current densities.

B concentration of the 20 mg/L. Biochar and A/char have little rhodamine B removal without  $\text{NaBH}_4$  (Fig. 5b). However, the  $\eta$  of A/char is large compared to biochar with  $\text{NaBH}_4$  (Fig. 5b). As Fig. 5b shown, the  $\eta$  of A/char without  $\text{NaBH}_4$  is lower than that of the A/char adding  $\text{NaBH}_4$ . Besides, when the rhodamine B solution only adds the  $\text{NaBH}_4$ , the  $\eta$  of the rhodamine B is low. These results prove that synergy between A/char and  $\text{NaBH}_4$  achieves the high rhodamine B removal. The main peak intensity of the rhodamine B gradually decreases with increasing in catalytic time (Fig. 5c). This phenomenon proves that rhodamine B molecular structure is ruined (Cheng et al., 2022). This result demonstrates that A/char has good rhodamine B catalytic performance.

#### 3.4.4. Energy storage of A/char

The energy storage potential of the A/char at 50–2000  $\text{mA g}^{-1}$  is presented in Fig. 6. The ratio of initial charge and discharge is 53.84% based on Fig. 6. Besides, the specific energy storage capacities are 350, 270, 220, 168, 140, 91 and 320  $\text{mAh g}^{-1}$  at 50–2000  $\text{mA g}^{-1}$ , respectively. Remarkably, the specific capacity is comparable to the first charge reversible capacity with the capacity retention of 91.43% when current density returns to 50  $\text{mA g}^{-1}$ . This result indicates that A/char has good reversibility. As Fig. 6 shown, A/char specific capacity is large at 50  $\text{mA g}^{-1}$  with 350  $\text{mAh g}^{-1}$ . It can be explained that Ag in A/char plays an important role in energy storage. Besides, A/char has layered structure created more free space and holes for volume changes, which is conducive to the transport of lithium ions due to large surface area.

## 4. Conclusions

Physicochemical properties of pyrolysis products are analyzed at 400–800 °C. High pyrolysis temperature contributes to the production of bio-gas and restrains the generation of biochar. However, bio-oil yield is little influenced by the pyrolysis temperature. Pyrolysis temperature influences the composition and heating value of bio-gas. The maximum heating value of bio-gas is 13.41  $\text{MJ/Nm}^3$ , which can provide energy for industrial production. Biochar is employed as the adsorbent for  $\text{Ag}^+$  removal, which forms A/char by reduction with the adsorp-

tion amount of the 65.14 mg/g at the concentration of 250 mg/L. The formed A/char is acted as the catalyst for rhodamine B degradation with the removal of the 81.75% at the 20 mg/L. The formed A/char is used in energy storage with the 350  $\text{mAh g}^{-1}$  at 50  $\text{mA g}^{-1}$ . Besides, the reduction process of the A/char is analyzed.

## Declaration of Competing Interest

The authors declare that they have no known competing financial interests or personal relationships that could have appeared to influence the work reported in this paper.

## Acknowledgments

The authors would like to express their gratitude to the Specialized Research Fund for the Natural Science Foundation of Henan Province (232300420298), the Fundamental Research Funds for the Universities of Henan Province (NSFRF220417) for financial support.

## Appendix A. Supplementary material

Supplementary data to this article can be found online at <https://doi.org/10.1016/j.arabjc.2023.105187>.

## References

- Abbas, Q., Yousaf, B., Ullah, H., Ali, M.U., Zia-ur-Rehman, M., Rizwan, M., Rinklebe, J., 2020. Biochar-induced immobilization and transformation of silver-nanoparticles affect growth, intracellular-radicals generation and nutrients assimilation by reducing oxidative stress in maize. *J. Hazard. Mater.* 390, 121976.
- Abdelsayed, V., Shekhawat, D., Smith, M.W., Link, D., Stiegman, A. E., 2018. Microwave-assisted pyrolysis of Mississippi coal: a comparative study with conventional pyrolysis. *Fuel* 217, 656–667.
- Al-Enizi, A.M., Ahmed, J., Ubaidullah, M., Shaikh, S.F., Ahamad, T., Naushad, M., Zheng, G., 2020. Utilization of waste polyethylene terephthalate bottles to develop metal-organic frameworks for energy applications: a clean and feasible approach. *J. Clean. Prod.* 248, 119251.
- Al-Enizi, A.M., Ubaidullah, M., Ahmed, J., Ahamad, T., Ahmad, T., Shaikh, S.F., Naushad, M., 2020. Synthesis of NiOx@NPC composite for high-performance supercapacitor via waste PET plastic-derived Ni-MOF. *Compos. Part B- Eng.* 183, 107655.
- Alshawi, J.M.S., Mohammed, M.Q., Alesary, H.F., Ismail, H.K., Barton, S., 2022. Voltammetric determination of  $\text{Hg}^{2+}$ ,  $\text{Zn}^{2+}$ , and  $\text{Pb}^{2+}$  ions using a PEDOT/NTA-modified electrode. *ACS Omega* 7 (23), 20405–20419.
- Aysu, T., Durak, H., 2015. Catalytic pyrolysis of liquorice (*Glycyrrhiza glabra* L.) in a fixed-bed reactor: Effects of pyrolysis parameters on product yields and character. *J. Anal. Appl. Pyrolysis* 111, 156–172.
- Cao, Y., Chen, S.S., Tsang, D.C., Clark, J.H., Zhang, S., 2020. Microwave-assisted depolymerization of various types of waste lignin over two-dimensional CuO/BCN catalysts. *Green Chem.* 22 (3), 725–736.
- Chen, P., Xie, Q., Addy, M., Zhou, W., Liu, Y., Wang, Y., Cheng, Y., Li, K., Ruan, R., 2016. Utilization of municipal solid and liquid wastes for bioenergy and bioproducts production. *Bioresour. Technol.* 215, 163–172.
- Cheng, S., Zhang, L., Xia, H., Peng, J., Shu, J., 2017. Adsorption behavior of methylene blue onto waste-derived adsorbent and exhaust gases recycling. *Rsc Adv.* 7, 27331–27341.



- Cheng, S., Xing, B.L., Shi, C.L., Nie, Y.H., Xia, H.Y., 2021. Efficient and selective removal of Pb(II) from aqueous solution by modification crofton weed: experiment and density functional theory calculation. *J. Clean. Prod.* 280, 124407.
- Cheng, S., Zhao, S.D., Xing, B.L., Shi, C.L., Meng, W.B., Zhang, C. X., Zhang, B., 2022. Facile one-pot green synthesis of magnetic separation photocatalyst-adsorbent and its application. *J. Water Process. Eng.* 47, 102802.
- Cheng, S., Meng, M.L., Xing, B.L., Shi, C.L., Nie, Y.H., Xia, D.P., Yi, G.Y., Zhang, C.X., Xia, H.Y., 2022. Preparation of valuable pyrolysis products from poplar waste under different temperatures by pyrolysis: evaluation of pyrolysis products. *Bioresour. Technol.* 364, 128011.
- Cheng, S., Meng, W.B., Xing, B.L., Shi, C.L., Wang, Q., Xia, D.P., Nie, Y.H., Zhang, C.X., Yi, G.Y., Xia, H.Y., 2023. Efficient removal of heavy metals from aqueous solutions by Mg/Fe bimetallic oxide-modified biochar: experiments and DFT investigations. *J. Clean. Prod.* 403, 136821.
- Cherubini, F., Ulgiati, S., 2010. Crop residues as raw materials for biorefinery systems – A LCA case study. *Appl. Energy* 87, 47–57.
- Foong, S.Y., Liew, R.K., Yang, Y., Cheng, Y.W., Yek, P.N.Y., Mahari, W.A.W., Lee, X.Y., Han, C.S., Vo, D.-V.-N., Quyet Van, L., Aghbashlo, M., Tabatabaei, M., Sonne, C., Peng, W., Lam, S. S., 2020. Valorization of biomass waste to engineered activated biochar by microwave pyrolysis: progress, challenges, and future directions. *Chem. Eng. J.* 389, 124401.
- Gautam, R., Shyam, S., Reddy, B.R., Govindaraju, K., Vinu, R., 2019. Microwave-assisted pyrolysis and analytical fast pyrolysis of macroalgae: product analysis and effect of heating mechanism. *Sustain. Energy Fuels* 3 (11), 3009–3020.
- Han, J.-A., Chung, H.-J., Lim, S.-T., 2019. Physical and emulsifying properties of OSA-corn dextrin with various manufacturing methods. *Food Hydrocolloid.* 89, 563–569.
- Hou, L., Xing, B., Zeng, H., Kang, W., Guo, H., Cheng, S., Huang, G., Cao, Y., Chen, Z., Zhang, C.X., 2022. Aluminothermic reduction synthesis of Si/C composite nanosheets from waste vermiculite as high-performance anode materials for lithium-ion batteries. *J. Alloy. Compd.* 922, 166134.
- Kabir, G., Din, A.T.M., Hameed, B.H., 2018. Pyrolysis of oil palm mesocarp fiber catalyzed with steel slag-derived zeolite for bio-oil production. *Bioresour. Technol.* 249, 42–48.
- KristinaMaljutina, T.A., JianglongYu, S.S.N., 2017. Comparative study on flash pyrolysis characteristics of microalgal and lignocellulosic biomass in entrained-flow reactor. *Energy Convers. Manage.* 151, 426–438.
- Li, H., Jiang, D., Huang, Z., He, K., Zeng, G., Chen, A., Yuan, L., Peng, M., Huang, T., Chen, G., 2019. Preparation of silver-nanoparticle-loaded magnetic biochar/poly (dopamine) composite as catalyst for reduction of organic dyes. *J. Colloid Interface Sci.* 555, 460–469.
- Mohammed, M.Q., Ismail, H.K., Alesary, H.F., Barton, S., 2022. Use of a Schiff base-modified conducting polymer electrode for electrochemical assay of Cd(II) and Pb(II) ions by square wave voltammetry. *Chem. Pap.* 76 (2), 715–729.
- Mukarakate, C., McBrayer, J.D., Evans, T.J., Budhi, S., Robichaud, D.J., Iisa, K., ten Dam, J., Watson, M.J., Baldwin, R.M., Nimlos, M.R., 2015. Catalytic fast pyrolysis of biomass: the reactions of water and aromatic intermediates produces phenols. *Green Chem.* 17, 4217–4227.
- Nishu, L.Y., Liu, R., 2022. Catalytic pyrolysis of lignin over ZSM-5, alkali, and metal modified ZSM-5 at different temperatures to produce hydrocarbons. *J. Energy Inst.* 101, 111–121.
- Parvez, A.M., Wu, T., Afzal, M.T., Mareta, S., He, T., Zhai, M., 2019. Conventional and microwave-assisted pyrolysis of gumwood: a comparison study using thermodynamic evaluation and hydrogen production. *Fuel Processing Technol.* 184, 1–11.
- Prashanth, P.F., Kumar, M.M., Vinu, R., 2020. Analytical and microwave pyrolysis of empty oil palm fruit bunch: kinetics and product characterization. *Bioresour. Technol.* 310, 123394.
- Qin, X., Cheng, S., Xing, B., Qu, X., Shi, C., Meng, W., Zhang, C., Xia, n.d. H., n et al.2023a. Preparation of pyrolysis products by catalytic pyrolysis of poplar: Application of biochar in antibiotic wastewater treatment and energy storage. *Chemosphere* 338, 139519.
- Qin, X.J., Zeng, X.W., Cheng, S., Xing, B.L., Shi, C.L., Yi, G.Y., Nie, Y.H., Wang, Q., Zhang, C.X., Xia, H.Y., 2023b. Preparation of double functional carbon-based ZnO derived from rape straw for dye wastewater treatment. *J. Water Process. Eng.* 52, 103588.
- Tang, Y.-H., Liu, S.-H., Tsang, D.C.W., 2020. Microwave-assisted production of CO<sub>2</sub>-activated biochar from sugarcane bagasse for electrochemical desalination. *J. Hazard. Mater.* 383, 121192.
- Ubaidullah, M., Al-Enizi, A.M., Ahamad, T., Shaikh, S.F., Al-Abdrabalnabi, M.A., Samdani, M.S., Kumar, D., Alam, M.A., Khan, M., 2021. Fabrication of highly porous N-doped mesoporous carbon using waste polyethylene terephthalate bottle-based MOF-5 for high performance supercapacitor. *J. Energy Storage* 33, 102125.
- Wang, Y., Dai, L., Wang, R., Fan, L., Liu, Y., Xie, Q., Ruan, R., 2016. Hydrocarbon fuel production from soapstock through fast microwave-assisted pyrolysis using microwave absorbent. *J. Anal. Appl. Pyrol.* 119, 251–258.
- Wang, Y., Akbarzadeh, A., Chong, L., Du, J., Tahir, N., Awasthi, M. K., 2022. Catalytic pyrolysis of lignocellulosic biomass for bio-oil production: a review. *Chemosphere* 297, 134181.
- Yang, Y., Liew, R.K., Tamothran, A.M., Foong, S.Y., Yek, P.N.Y., Chia, P.W., Tran, T.V., Peng, W., Lam, S.S., 2021. Gasification of refuse-derived fuel from municipal solid waste for energy production: a review. *Environ. Chem. Lett.* 19, 2127–2140.
- Yek, P.N.Y., Chen, X., Peng, W., Liew, R.K., Cheng, C.K., Sonne, C., Sii, H.S., Lam, S.S., 2021. Microwave co-torrefaction of waste oil and biomass pellets for simultaneous recovery of waste and co-firing fuel. *Renew. Sust. Energ. Rev.* 152, 111699.
- Yek, P.N.Y., Cheng, Y.W., Liew, R.K., Mahari, W.A.W., Ong, H.C., Chen, W.-H., Peng, W., Park, Y.-K., Sonne, C., Kong, S.H., Tabatabaei, M., Aghbashlo, M., Lam, S.S., 2021. Progress in the torrefaction technology for upgrading oil palm wastes to energy-dense biochar: a review. *Renew. Sust. Energ. Rev.* 151, 111645.
- Zhang, X., Che, Q., Cui, X., Wei, Z., Zhang, X., Chen, Y., Wang, X., Chen, H., 2018. Application of biomass pyrolytic polygeneration by a moving bed: characteristics of products and energy efficiency analysis. *Bioresour. Technol.* 254, 130–138.
- Zhang, Y., Chen, P., Liu, S., Peng, P., Min, M., Cheng, Y., Anderson, E., Zhou, N., Fan, L., Liu, C., 2017. Effects of feedstock characteristics on microwave-assisted pyrolysis - A review. *Biore-sour. Technol.* 230, 143–151.
- Zhang, S., Ji, Y., Dang, J., Zhao, J., Chen, S., 2019. Magnetic apple pomace biochar: Simple preparation, characterization, and application for enriching Ag(I) in effluents. *Sci. Total Environ.* 668, 115–123.
- Zhang, B., Yang, C., Moen, J., Le, Z., Hennessy, K., Wan, Y., Liu, Y., Lei, H., Chen, P., Ruan, R., 2010. Catalytic conversion of microwave-assisted pyrolysis vapors. *Energy Sources Part A* 32, 1756–1762.
- Zhao, T., Yao, Y., Li, D., Wu, F., Zhang, C., Gao, B., 2018. Facile low-temperature one-step synthesis of pomelo peel biochar under air atmosphere and its adsorption behaviors for Ag(I) and Pb(II). *Sci. Total Environ.* 640, 73–79.